Research Article

Shumin Du, Huaiyin Chen, and Ruoyu Hong*

Preparation and electromagnetic properties characterization of reduced graphene oxide/strontium hexaferrite nanocomposites

https://doi.org/10.1515/ntrev-2020-0010
Received Dec 02, 2019; accepted Dec 16, 2019

Abstract: With the rapid development of electronics and information technology, electronics and electrical equipment have been widely used in our daily lives. The living environment is full of electromagnetic waves of various frequencies and energy. Electromagnetic wave radiation has evolved into a new type of environmental pollution that has been listed by the WHO (World Health Organization) as the fourth largest source of environmental pollution after water, atmosphere, and noise. Studies have shown that when electromagnetic wave radiation is too much, it can cause neurological disorders. And electromagnetic interference will cause the abnormal operation of medical equipment, precision instruments and other equipment, and therefore cause incalculable consequences. Therefore, electromagnetic protection has become a hot issue of concern to the social and scientific circles.

Keywords: Strontium hexaferrite, Reduced graphene oxide, Electromagnetic properties

1 Introduction

At present, countries around the world have increased their research on the problem of electromagnetic wave pollution, and have successively formulated relevant standards and regulations to control and purify the electromagnetic environment [1, 2]. The most effective measure to control electromagnetic radiation pollution is electromagnetic shielding to control its radiation intensity within a safe range [3, 4]. Absorbing material refers to the ability to convert electromagnetic waves into other forms of energy such as thermal energy, electrical energy, or mechanical energy through its own absorption effect so that electromagnetic waves are consumed or attenuated [5]. The frequency range of absorbing materials is very wide. The frequency band is from 100 MHz to 300 GHz. The frequency range of 2 to 18 GHz is the most widely used. Therefore, the research focus of absorbing materials in recent years is in this frequency range [6]. Excellent electromagnetic matching performance and high strength loss ability are indispensable conditions for the absorbing material to effectively absorb electromagnetic waves [7]. Besides, it meets the design requirements for modern electromagnetic absorbing materials with thin thickness, absorption frequency bandwidth, strong absorbing performance, and light weight. However, single absorbing material cannot meet all the performance requirements of "thin, light, wide and strong" of absorbing materials. Therefore, two or more materials are usually compounded, and the structure is meticulously designed to maximize the electromagnetic absorption performance.

RGO has a large number of residual oxygen-containing functional groups on its surface, such as hydroxyl, carboxyl, carbonyl, and epoxy groups, which can cause defects such as defect polarization and electron dipole relaxation [8]. RGO possesses the advantages of large specific surface area, high dielectric constant, and light weight, which make it exhibit a certain microwave absorption performance [9]. However, the overall attenuation effect of single RGO on electromagnetic waves is still relatively weak. Ferrite, as a dual-composite material, can generate both magnetic loss and dielectric loss, so it has good electromagnetic properties [10], but single ferrite has a higher density. The combination of RGO and ferrite to form complementary advantages: On the one hand, it has both magnetic loss and electrical loss, which is beneficial to achieve electromagnetic matching and improve absorbing performance; On the other hand, it is beneficial to reduce the density of the absorbing material [11]. Zheng *et al.* synthesized Fe_3O_4-graphene composites, which has hydrophobicity and superparamagnetism. The results show that the maximum reflection loss is −40 dB at a frequency of 6.8

***Corresponding Author: Ruoyu Hong:** College of Chemical Engineering, Fuzhou University, Fuzhou 350116, China;
Email: rhong@fzu.edu.cn, Tel/Wechat: 18859199060
Shumin Du, Huaiyin Chen: College of Chemical Engineering, Fuzhou University, Fuzhou 350116, China

GHz and a matching thickness of 4.5 mm is 4.6–18 GHz [12]. Shu *et al.* prepared RGO/MWCNTs/$ZnFe_2O_4$ nanocomposites by a simple one-pot hydrothermal method, which has a three-dimensional conductive network structure. When the mass ratio of GO to MWCNTs is 1:1, at a thickness of 5mm, the maximum reflection loss was −23.8 dB and the effective absorption bandwidth was 2.6 GHz [13].

In spite of many reports on composites of RGO and ferrite for microwave absorption, there have been few reports in China about RGO/$SrFe_{12}O_{19}$ nanocomposite as highfrequency microwave absorber up to now. $SrFe_{12}O_{19}$ ferrite has large saturation magnetization [14], excellent coercivity [15], high uniaxial magnetocrystalline anisotropy [16], excellent electromagnetic properties [17], chemical stability and corrosion resistance [18] that plays an important role in hard magnetic materials. The combination of RGO/$SrFe_{12}O_{19}$ maybe has great application potential in the field of microwave absorbing materials [19]. In this work, we prepared the RGO/$SrFe_{12}O_{19}$ nanocomposites by a one-step hydrothermal reaction with the assistance of the EG. The morphology, phase structure, magnetic properties, electromagnetic properties and absorption performance of the prepared nanocomposites were investigated in detail.

2 Materials and methods

2.1 Materials

Ferric chloride hexahydrate ($FeCl_3 \cdot 6H_2O$), absolute ethyl alcohol, ethylene glycol ($C_2H_6O_2$), hydrochloric acid (HCl) and sodium hydroxide (NaOH), buy from Sinopharm Chemical Reagent Co. Ltd. Strontium chloride hexahydrate ($SrCl_2 \cdot 6H_2O$) was purchased from Aladdin. All chemicals used during the experiment were reagent grade. Ultrapure water was used throughout the experiment.

2.2 Prepared of RGO/$SrFe_{12}O_{19}$ nanocomposites

GO was prepared through a modified Hummers method that natural graphite flakes is oxidized by strong oxidant, then treated at high temperature [20]. 0.11 g of GO was dispersed in the mixture of ethylene glycol and deionized water (35mL of ethylene glycol+15mL of deionized water) by ultrasonication for 30 min. Then 0.49 g of $SrCl_2 \cdot 6H_2O$ and 4 g of $FeCl_3 \cdot 6H_2O$ were dissolved into GO suspension. 20 mL of NaOH aqueous solution was added to the iron salt solution by a peristaltic pump until the pH value reached to 13. The suspension of precursors was heated to 80°C with vigorous mechanical stirring for 30 min, and then transferred into a 100 mL teflon-lined stainless steel autoclave and heated to 200°C in a blast drying oven, and the reaction was held for 12 hours. Cooled naturally to room temperature, magnetically separate, washed with ultrapure water until the pH reached to 13, washed with HCl (the purpose is to remove excess strontium carbonate), then washed with ultrapure water and ethyl alcohol and finally dried in a vacuum oven at 60°C for 24 h.

2.3 Characterization

The transmission electron microscope (TEM, TF20, Jeol 2100F) was used to characterize the micro-morphology of nanocomposites. The crystal structure was characterized by X-ray powder diffractometer (XRD, DY5261/Xpert3, CEM, USA), using a Cu target (λ = 1.5418 Å), test range is 5-80°. The magnetic properties of the product were tested using a vibrating sample magnetometer (VSM-7400, Lake Shore, USA) at room temperature with a magnetic field strength of 30,000 Oe. The vector network analyzer (VNA, PNA-A5244A) was used to measure the real (ε') and imaginary parts (ε'') of the complex permittivity and the real (μ') and imaginary parts (μ'') of the complex permeability in the frequency range of 2 to 18 GHz. The samples were prepared by mixing the RGO/$SrFe_{12}O_{19}$ nanocomposites with paraffin in a mass ratio of 7: 3 and pressing it into a ring (φ_{in} = 3.04 mm, φ_{out} = 7 mm). Then used Matlab to calculate the reflection loss of the samples and analyze the change in electromagnetic absorption performance.

3 Results and discussion

3.1 Morphological and structural characterization of samples

Figure 1 shows the TEM images of representative $SrFe_{12}O_{19}$ nanoparticles and RGO/$SrFe_{12}O_{19}$ nanocomposites. It can be seen from Figure 1a that $SrFe_{12}O_{19}$ is a flaky structure, the particle size is mainly distributed at 8-15 nm. In addition, the particles have a certain degree of agglomeration, which is related to the magnetic dipole interaction between the nanoparticles. It can be seen from Figure 1b that the $SrFe_{12}O_{19}$ nanoflakes are uniformly supported on the RGO nanosheets, and there is almost no agglomeration and exhibit better dispersibil-

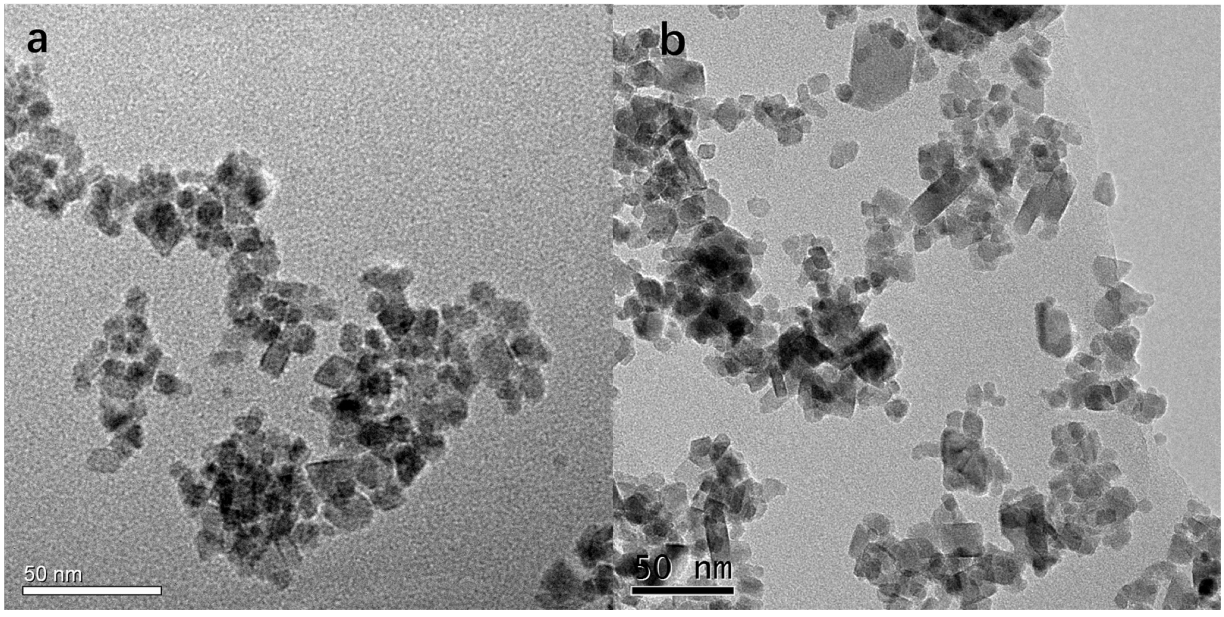

Figure 1: TEM images of (a) $SrFe_{12}O_{19}$ nanoparticles and (b) RGO/$SrFe_{12}O_{19}$

ity than pure $SrFe_{12}O_{19}$ nanoparticles. That is mainly because $SrFe_{12}O_{19}$ nanoflakes are coated with graphene with pleated structure, which hinders the volume change of $SrFe_{12}O_{19}$ nanoparticles, and prevents the detachment and agglomeration of the $SrFe_{12}O_{19}$ nanoparticles. The prepared RGO/$SrFe_{12}O_{19}$ nanocomposite material has a small particle size, which has a small size effect, surface effect, lattice distortion, multiple exchange coupling effects between nanocrystals, etc., and has a large hysteresis loss, thereby exhibiting good electromagnetic wave absorption capabilities.

The phase and crystal structure of the $SrFe_{12}O_{19}$ nanoflakes and RGO/$SrFe_{12}O_{19}$ nanocomposites were studied by XRD, confirmed by the standard JCPDS card (PDF # 84-1531) [21]. The positions of the diffraction peaks of $SrFe_{12}O_{19}$ nanoparticles and RGO/$SrFe_{12}O_{19}$ nanocomposites are basically the same, indicating that the addition of RGO has no effect on the crystal form of the composite. The significant peaks at 2θ values of 30°, 33°, 35.4°, 40.9°, 43.6°, 49.5°, 54°, 57.2° and 62.2° were assigned to (110), (107), (114), (205), (206), (209), (217), (2011) and (220) planes [22]. The results show that all diffraction peaks correspond to the face-centered cubic structure of $SrFe_{12}O_{19}$ in the literature [23]. As can be seen from Figure 2, all the diffraction peaks are sharp and narrow, indicating that the $SrFe_{12}O_{19}$ nanoparticles are highly crystalline. We can see that the characteristic peak of (001) of graphene oxide around $2\theta = 10°$ on GO completely disappeared on the RGO/$SrFe_{12}O_{19}$ nanocomposites spectrum, indicating that the degree of reduction of GO was quite high during the entire reaction process [24]. In addition, no diffraction peak was observed around 26°, indicating that RGO nanosheets are dispersed uniformly and do not overlap [9]. The results provide an evidence that the composites of GO and $SrFe_{12}O_{19}$ have been successfully combined together to form a composite after reaction.

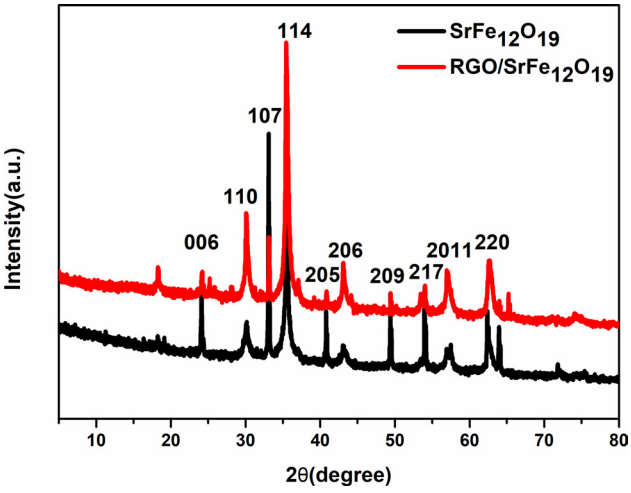

Figure 2: XRD patterns of $SrFe_{12}O_{19}$ nanoparticles and RGO/$SrFe_{12}O_{19}$ nanocomposites

3.2 Magnetic properties

Figure 3 displays the hysteresis loops of $SrFe_{12}O_{19}$ nanoparticles and RGO/$SrFe_{12}O_{19}$ nanocomposites, re-

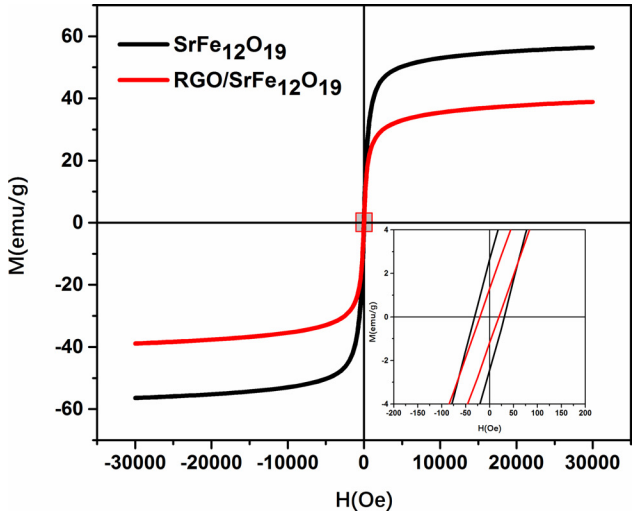

Figure 3: Magnetic hysteresis loops for $SrFe_{12}O_{19}$ nanoparticles and RGO/$SrFe_{12}O_{19}$ nanocomposites

spectively. It is clear that the two samples have the same hysteresis behavior. The $SrFe_{12}O_{19}$ nanoparticles and RGO/$SrFe_{12}O_{19}$ nanocomposites are superparamagnetic, indicating that the nanocrystals are small in size. The saturation magnetization (Ms) of RGO/$SrFe_{12}O_{19}$ nanocomposites (38.8 emu/g) is smaller than that of $SrFe_{12}O_{19}$ nanoparticles (56.3 emu/g), due to the addition of nonmagnetic RGO, which causes a magnetic dilution effect. It can be found that the remanent magnetization (Mr) and coercivity (Hc) are about 2.7 emu/g and 31.0 Oe for $SrFe_{12}O_{19}$ nanoparticles, 1.3 emu/g and 20 Oe for RGO/$SrFe_{12}O_{19}$ nanocomposites, respectively. The addition of RGO has no effect on the coercive force of the $SrFe_{12}O_{19}$ nanoparticles. The reason for the low coercive force value is the large shape anisotropy of the sample. This higher value of anisotropy energy makes the nanocomposite a good candidate for the development of electromagnetic absorption properties [25].

3.3 Analysis of electromagnetic parameters

Figure 4 shows the electromagnetic parameters of $SrFe_{12}O_{19}$ nanoparticles and RGO/$SrFe_{12}O_{19}$ nanocomposites. The real part (ε') and imaginary part (ε'') of the complex permittivity represent the storage and consumption capacity of electric energy, and the real part (μ') and imaginary part (μ'') of the complex permeability represent the storage of magnetic energy and consumption [26]. The ε' and ε'' are shown in Figure 4. As can be seen, the ε' of the RGO/$SrFe_{12}O_{19}$ nanocomposites gradually decreases from 18 to 12.6 in the range of 2-18 GHz, and the ε' of $SrFe_{12}O_{19}$ nanoparticles is relatively small and is almost constant at about 6.9 in the entire frequency range. The ε'' of RGO/$SrFe_{12}O_{19}$ nanocomposites is also much higher than that of $SrFe_{12}O_{19}$ nanoparticles. Over the entire frequency range, the ε'' value of RGO/$SrFe_{12}O_{19}$ nanocomposite exhibited three high fluctuations from 4.0 to 5.3, while the ε'' value of $SrFe_{12}O_{19}$ nanoparticles increases from 0.7 to 1.0. The results indicate that $SrFe_{12}O_{19}$ has a poor dielectric loss ability, but the dielectric loss performance is greatly improved in the presence of RGO. From the formula $\varepsilon'' \approx 1/2\pi\varepsilon_0\rho f$, it can be known that due to the addition of RGO, the electrical conductivity of the composite material increases, so that the resistivity of the material decreases and the dielectric loss increases [27]. As the XRD results show, the GO is reduced to RGO during the preparation process, and the conductivity increases, which enhancing its space charge polarization. In addition, the interfacial polarization is also a very important reason in that regards. $SrFe_{12}O_{19}$ and RGO have different intrinsic dielectric feature, thus, there are considerable charges accumulation at their interfaces [28, 29]. Under the action of an external electric field, the free charge between $SrFe_{12}O_{19}$ and RGO changes and jumps continuously, which results in polarization loss at the interface, thereby dissipating incident electromagnetic waves.

Figure 4c presents the real part of the relative complex permeability (μ'). It can be seen that the values of μ' of $SrFe_{12}O_{19}$ nanoparticles and RGO/$SrFe_{12}O_{19}$ nanocomposites have similar tendency for variation with frequency, and the μ' value decrease gradually in the range of 2-5.8 GHz, and changed little around 0.94 in the range of 5.8-18 GHz. This shows that the addition of RGO has little effect on the value of μ'. Figure 4d gives the imaginary part of the relative complex permeability (μ''). Both the $SrFe_{12}O_{19}$ nanoparticles and RGO/$SrFe_{12}O_{19}$ nanocomposites have gradually decreased across the entire frequency range, declining from 0.35 and 0.6 to 0 and −0.06, respectively. A negative value of μ'' at the frequencies greater than 14GHz, is considered to be the emission of electromagnetic energy from the absorbing material to the outside, which is caused by the electrical properties of the nanocomposites. Under the action of an alternating magnetic field, free electrons form a catastrophic flow due to Lorentz force, and then an eddy current generates an induced magnetic field. $SrFe_{12}O_{19}$ and RGO therefore form a conductive network. Part of the electric field energy is converted into magnetic field energy and released, whch is conducive to the material's absorbing performance.

In order to better study the electromagnetic properties of the $SrFe_{12}O_{19}$ nanoparticles and RGO/Fe_3O_4 nanocomposites, the tangent angle of dielectric loss ($\tan\delta_\varepsilon = \varepsilon''/\varepsilon'$)

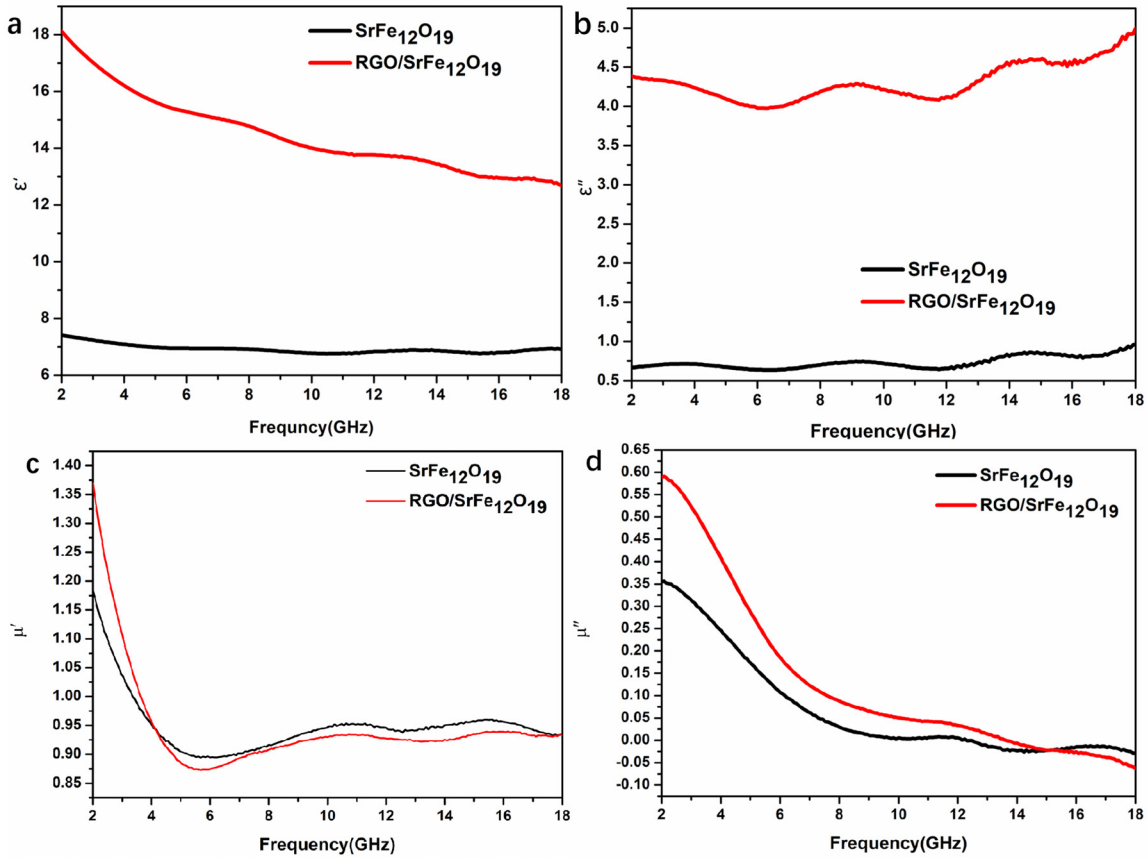

Figure 4: Frequency dependence of (a) real part of permittivity (ε'); (b) imaginary part of permittivity (ε''); (c) real part of permeability (μ'); (d) imaginary part of permeability (μ'') of $SrFe_{12}O_{19}$ nanoparticles and RGO/$SrFe_{12}O_{19}$ nanocomposites

and tangent angle of magnetic loss ($\tan\delta_\mu = \mu''/\mu'$) are calculated [30]. It can be seen from Figure 5a that the electrical loss $\tan\delta_\varepsilon$ of RGO/$SrFe_{12}O_{19}$ nanocomposites and $SrFe_{12}O_{19}$ nanoparticles are increased from 0.24 to 0.39 and 0.09 to 0.13 in the range 2-18 GHz. Compared with the $SrFe_{12}O_{19}$ nanoflakes, the $\tan\delta_\varepsilon$ of RGO/Fe_3O_4 nanocomposites are higher. The addition of a small amount of GO can greatly improve the dielectric loss capacity of the composite material, which is not only related to the conductive ability of RGO, but also related to the polarization process and electrical conductivity between the composite materials [31]. It can be clearly seen from Figure 5b that the $\tan\delta_\mu$ values of $SrFe_{12}O_{19}$ nanoparticles and RGO/$SrFe_{12}O_{19}$ nanocomposites both show similar trends with frequency. The $\tan\delta_\mu$ values decrease sharply in the range of 2-9 GHz, and remain basically unchanged within 9-18 GHz. The $\tan\delta_\mu$ values of $SrFe_{12}O_{19}$ nanoparticles are larger than that of the RGO/$SrFe_{12}O_{19}$ nanocomposites in the whole frequency range. By comparing the dielectric loss and magnetic loss of the RGO/$SrFe_{12}O_{19}$ nanocomposites, it is found that the absorbing performance of the RGO/$SrFe_{12}O_{19}$ nanocomposites is mainly a magnetic loss type ($\tan\delta_\mu > \tan\delta_\varepsilon$) in the frequency range of 2-5.5 GHz; the absorbing performance of the composite mainly shows the dielectric loss type ($\tan\delta_\varepsilon > \tan\delta_\mu$) in the frequency range of 2-5.5 GHz.

The effect of magnetic loss on electromagnetic wave absorption is very important. The electromagnetic energy is converted to thermal energy by magnetic loss to enhance electromagnetic wave absorption. Generally, in the low frequency range, the eddy current effect, hysteresis effect, and post-magnetism effect are the main causes of the attenuation loss of ferrites to electromagnetic waves; in the high frequency range, domain wall resonance loss, natural resonance loss, and dielectric loss is the main reason for the attenuation of electromagnetic waves by ferrites [32]. If only the eddy current loss is considered, the eddy current coefficient C_0 can be expressed as [33]:

$$C_0 = \mu^{\bullet}(\mu')^{-2}f^{-1} \quad (1)$$

Where the C_0 would be a constant, independent of the frequency. If the magnetic loss is generated from the eddy current effect, the C_0 will keep constant as the frequency varies [30]. Figure 5c shows the C_0 curves of

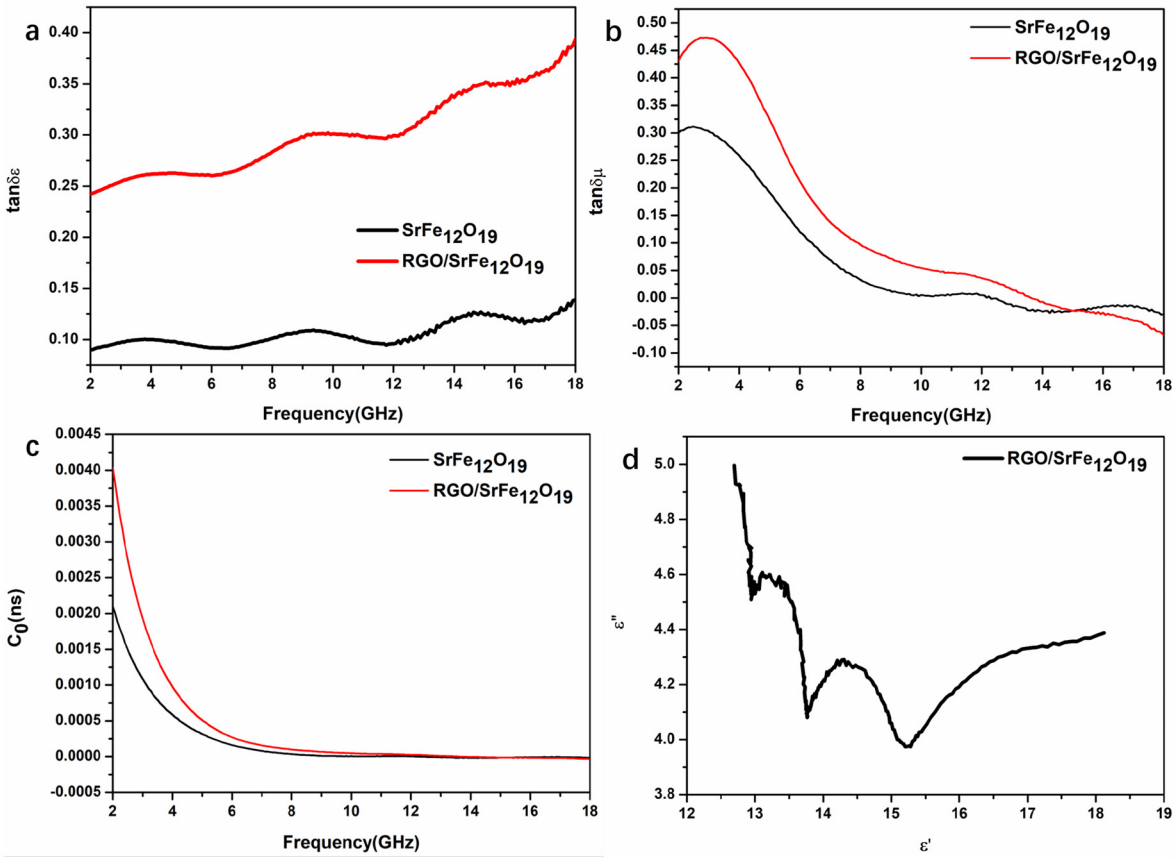

Figure 5: Frequency dependence of (a) dielectric loss factor (tan $\delta\varepsilon$); (b) magnetic loss factor (tan $\delta\mu$); (c) C_0 values of $SrFe_{12}O_{19}$ nanoparticles and RGO/$SrFe_{12}O_{19}$ nanocomposites; (d) Cole-Cole semicircle (ε'' versus ε') of RGO/$SrFe_{12}O_{19}$ nanocomposites

RGO/$SrFe_{12}O_{19}$ nanocomposites. while the C_0 is basically unchanged above 9 GHz, while above 9 GHz the C_0 is basically unchanged [34, 35]. This implies that the main reasons for the magnetic loss are natural resonance, hysteresis effect and exchange resonance in the range of 2-9 GHz, but eddy current loss accounts for the magnetic loss in the range of 9-18 GHz.

Dielectric relaxation has a great impact on the electromagnetic absorbing properties of nanocomposites. The relaxation phenomenon refers to a system in equilibrium, when it is affected by external force, the system shifts from its original equilibrium position. If the external force is removed. The system deviating from the original equilibrium position will return to the original equilibrium state. Debye's equation is the simplest equation to deal with polarization relaxation [36, 37]:

$$\left[\varepsilon' - \frac{1}{2}(\varepsilon_s + \varepsilon_\infty)^2\right] + (\varepsilon'')^2 = \frac{1}{4}(\varepsilon_s + \varepsilon_\infty)^2 \qquad (2)$$

Where ε_∞ is the limit value of the dielectric constant at high frequencies and ε_s is the static permittivity. The ε' and ε'' are two important physical quantities used to describe the relaxation process. Based on Equation 2, it can be seen that the relationship between ε' and ε'' is a semicircle with ε' as the abscissa and ε'' as the ordinate, which is called Debye semicircle, and each Debye semicircle represents a a Debye relaxation process [34]. The $\varepsilon''-\varepsilon'$ curves of RGO/$SrFe_{12}O_{19}$ nanocomposites are shown in Figure 5d. It can be clearly seen that there are three distinct Cole-Cole semicircles in the $\varepsilon'' - \varepsilon'$ curve of the RGO/$SrFe_{12}O_{19}$ nanocomposite. The results show that there are three effective Debye relaxation processes in the RGO/$SrFe_{12}O_{19}$ nanocomposites. There are two main reasons for the relaxation process: the first is due to the interfacial polarization between $SrFe_{12}O_{19}$ and RGO; the second is that the surface of RGO contains a large number of residual defects and functional groups [38]. It is worth noting that the Cole-Cole semicircle of the composite is irregular, which indicates that in addition to the Debye relaxation of the composite, there are also influencing factors, such as dipolar polarization, electron polarization, Interfacial polarization and Maxwell-Wagner relaxation [39]. Eventually lead to absorption and attenuation of electromagnetic wave energy, and improving the electromagnetic wave absorbing performance of RGO/$SrFe_{12}O_{19}$ nanocomposites.

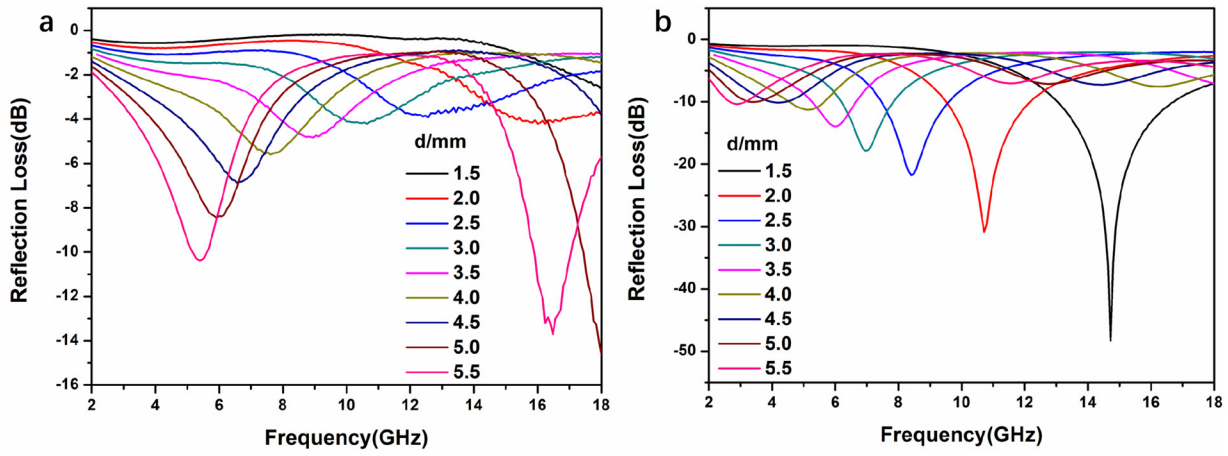

Figure 6: RL of (a) $SrFe_{12}O_{19}$ nanoflakes; (b) RGO/$SrFe_{12}O_{19}$ nanocomposites

3.4 Analysis of absorbing properties

The ideal absorbing material can completely absorb and lose electromagnetic waves. It needs to meet the following two requirements [40]. First, the impedance matching characteristics of the absorbing material, that is, the impedance of the absorbing material and the impedance of the propagation medium are required to be as close as possible, so that the reflection coefficient of the interface between the material and the air is zero, and the electromagnetic wave energy in the air enters the material at most. On the other hand, when the electromagnetic wave enters the material as much as possible, the absorbing material should also have good attenuation characteristics, that is, the electromagnetic wave entering the material is maximized by the loss.

The absorbing material requires a low reflectivity and also requires a frequency bandwidth. Its absorption of electromagnetic waves is evaluated by reflection loss (RL), For single-layer absorbers, RL is given by the the following formula [41, 42]:

$$RL(dB) = 20\log\left|(Z_{in} - Z_0)/(Z_{in} - Z_0)\right| \quad (3)$$

$$Z_{in} = Z_0\left(\mu_r/\varepsilon_r\right)^{1/2}\tanh\left[j\left(2\pi fd\left(\mu_r\varepsilon_r\right)^{1/2}/c\right)\right] \quad (4)$$

Where Z_{in} and Z_0represents the wave impedance of the absorbing material and the wave impedance of the air; μ_r and ε_r are the relative permeability and relative permittivity of the nanomaterials; f is the frequency; d represents the thickness of the absorbing material; and c represents the speed of light ($3{\cdot}10^8$ m/s).

Figure 6a-b displays the RL of $SrFe_{12}O_{19}$ nanoparticles and RGO/$SrFe_{12}O_{19}$ nanocomposites at 2-18 GHz, respectively. The RL of the RGO/$SrFe_{12}O_{19}$ nanocomposites is significantly improved compared to that of $SrFe_{12}O_{19}$ nanoparticles. At thickness of 1.5 mm, the maximum RL of RGO/$SrFe_{12}O_{19}$ nanocomposites is −48.1 dB with effective absorption bandwidth of 3.9 GHz (12.9-16.8 GHz). For $SrFe_{12}O_{19}$ nanoparticles, the maximum RL appears at 16.4 GHz up to −13.5 dB under 5.5 mm thickness, with the bandwidth below −10 dB ranging from 16 to 17 GHz. It shows that adding a small amount of RGO greatly affects the dielectric loss and magnetic loss, and greatly improves the microwave absorption performance of RGO/$SrFe_{12}O_{19}$ nanocomposites.

Figure 7 exhibits the three-dimensional presentations of the calculated RL curves and the two-dimensional image maps of RL of the RGO/$SrFe_{12}O_{19}$ nanocomposites. According to the International Radiation Protection Association (IRPA), when the RL < −10 dB, the material's electromagnetic wave absorption rate reaches 90%, then the material has wave absorbing performance [43]. Therefore, the frequency band of the absorbing material's reflection loss value below −10 dB should be as wide as possible in order to absorb more electromagnetic waves in the frequency range [44]. Obviously, when the thickness is changed in the range of 1.5-5.5 mm, the effective absorption band reaches 16 GHz (from 2 GHz-18 GHz). The results show that it is crucial to adjust the thickness of the nanocomposite for application at different frequencies. By comparing the positions of the reflection loss peaks of composite materials with different thicknesses, it can be found that as the thickness of the material increases, the position of the reflection loss peak moves to a lower frequency band and the peak value decreases. Therefore, in practical applications, different microwave absorption bands should be selected with appropriate thicknesses.

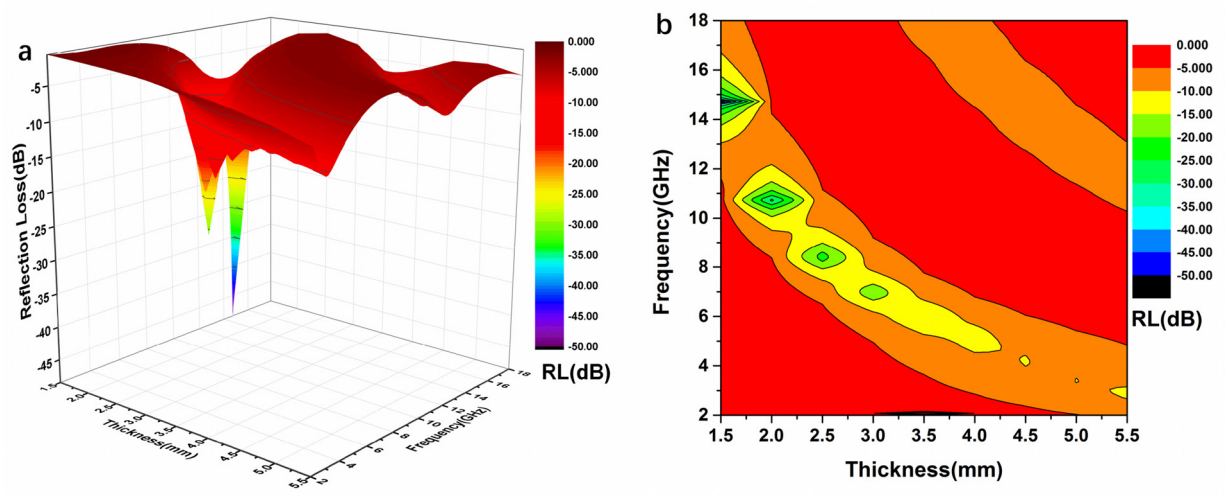

Figure 7: (a) 3D representation of RL performance of RGO/$SrFe_{12}O_{19}$ nanocomposites; (b) Contours of the calculated RL values for RGO/$SrFe_{12}O_{19}$ nanocomposites

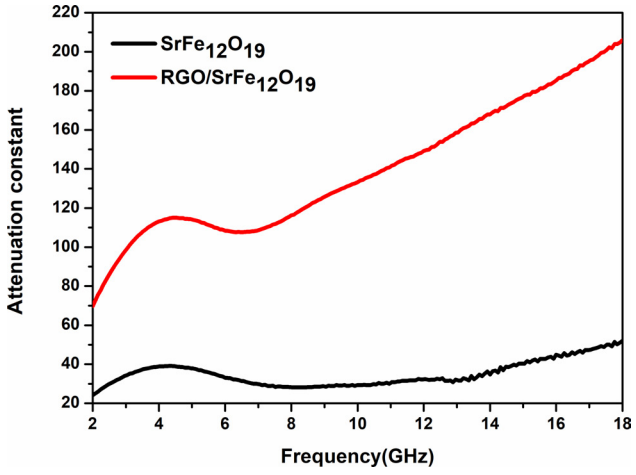

Figure 8: Attenuation constant α of the as-prepared RGO/$SrFe_{12}O_{19}$ nanocomposites

The value of the attenuation constant α represents the strength of the material's ability to lose electromagnetic waves. The larger the value of α, the stronger the material's ability to absorb electromagnetic waves. α obeys the following formula [45, 46]:

$$\alpha = \frac{\sqrt{2}\pi f}{c} \times \sqrt{(\mu''\varepsilon'' - \mu'\varepsilon') + \sqrt{(\mu''\varepsilon'' - \mu'\varepsilon')^2 (\varepsilon'\mu'' + \varepsilon''\mu')^2}} \quad (5)$$

Figure 8 shows the curve of attenuation constant α changing with frequency. It can be found that the α value of the RGO/$SrFe_{12}O_{19}$ nanocomposites is much larger than the $SrFe_{12}O_{19}$ nanoparticles in the entire frequency range. It shows that the material has more excellent attenuation performance, which is consistent with the dielectric loss results. Adding an appropriate amount of RGO can increase the dielectric loss of the RGO/$SrFe_{12}O_{19}$ nanocomposite material, thereby improving impedance matching and facilitating incident microwaves to enter the composite material. All these also help to enhance microwave absorption in composites.

4 Conclusions

In summary, the RGO/$SrFe_{12}O_{19}$ have been successfully prepared by using EG assisted hydrothermal synthesis. The results show a good synergy between the magnetic properties of $SrFe_{12}O_{19}$ and the dielectric properties of RGO. Compared with $SrFe_{12}O_{19}$ nanoparticles, the RGO/$SrFe_{12}O_{19}$ nanocomposites have the characteristics of light specific gravity, absorbing frequency bandwidth, adjustable electromagnetic parameters, and large absorbing loss. The maximum RL of RGO/$SrFe_{12}O_{19}$ nanocomposites with the thickness of 1.5 mm reached −48.1 dB at 14.7 GHz, and the bandwidth of RL less than −10 dB ranged from 12.9 to 16.8 GHz.

Acknowledgement: This research was financially supported by Minjiang Scholarship of Fujian Province (No. Min-Gaojiao[2010]-117), Central-government Guided Fund for Local Economic Development (No. 830170778), R&D Fund for Strategic Emerging Industry of Fujian Province (No. 82918001), International Cooperation Project of Fujian Science and Technology Department (No. 830170771) and Teaching and Researching Fund for Young Staff of Fujian Educational Department (No. JT180040).

References

[1] Gao J., Luo J., Wang L., Huang X., Wang H., Song X., Hu M., Tang L.C., Xue H., Flexible, superhydrophobic and highly conductive composite based on non-woven polypropylene fabric for electromagnetic interference shielding, Chem. En. J., 2019, 364, 493-502.

[2] Ali A., Phull A.R., Zia M., Elemental zinc to zinc nanoparticles: is ZnO NPs crucial for life? Synthesis, toxicological, and environmental concerns, Nanotechnol. Rev., 2018, 7(5), 413-441.

[3] Chen C., Hou X., Si J.H., Design of an integrated optics for transglutaminase conformational change, Nanotechnol. Rev., 2018, 7(4), 283-290.

[4] Zhang H., Wang B., Feng A., Zhang N., Jia Z., Huang Z., Liu X., Wu G., Mesoporous carbon hollow microspheres with tunable pore size and shell thickness as efficient electromagnetic wave absorbers, Compos. Part. B-Eng., 2019, 167, 690-699.

[5] Zhang Y., Huang Y., Zhang T.F., Chang H.C., Xiao P.S., Chn H.H.; Huang Y., Chen Y.S., Broadband and tunable high-performance microwave absorption of an ultralight and highly compressible graphene foam, Adv. Mater., 2017, 6(6), 505-516.

[6] Wang Y., Gao X., Lin C., Shi L., Li X., Wu G., Metal organic frameworks-derived Fe-Co nanoporous carbon/graphene composite as a high-performance electromagnetic wave absorber, J. Alloys Compd., 2019, 785, 765-773.

[7] Wang Y.M., Pan M., Liang X.Y., Li B.J., Zhang S., Electromagnetic wave absorption coating material with self-healing properties, Macromol. Rapid Commun., 2017, 38(23), 1700447.

[8] Yu H.G., Chu C.L., Chu P.K., Self-assembly and enhanced visible-light-driven photocatalytic activity of reduced graphene oxide-Bi_2WO_6 photocatalysts, Nanotechnol. Rev., 2017, 6(6), 505-516.

[9] Zhang B., Li C.Y., Kuang W.C., Zhang J.X., Xiong Y.Q., Tan S.Z., Cai X., Huang L.H., Carboxymethyl cellulose-grafted graphene oxide for efficient antitumor drug delivery, Nanotechnol. Rev., 2018, 7 (4), 291-301.

[10] Zhang R., Huang X., Zhong B., Xia L., Wen G., Zhou Y., Enhanced microwave absorption properties of ferroferric oxide/graphene composites with a controllable microstructure, RSC Adv., 2016, 6 (21), 16952-16962.

[11] Zhao C., Shen M., Li Z., Sun R., Xia A., Liu X., Green synthesis and enhanced microwave absorption property of reduced graphene oxide-$SrFe_{12}O_{19}$ nanocomposites, J. Alloys Compd., 2016, 689, 1037-1043.

[12] Zheng X., Feng J., Zong Y., Miao H., Hu X., Bai J., Li X., Hydrophobic graphene nanosheets decorated by monodispersed superparamagnetic Fe_3O_4 nanocrystals as synergistic electromagnetic wave absorbers, J. Mater. Chem. C., 2015, 3 (17), 4452-4463.

[13] Shu R.W., Li W.J., Zhou X., Tian D.D., Zhang G.Y., Gan Y., Shi J.J., He J., Facile preparation and microwave absorption properties of RGO/MWCNTs/$ZnFe_2O_4$ hybrid nanocomposites, J. Alloys Compd., 2018, 743, 163-174.

[14] Ban I., Stergar J., Maver U., NiCu magnetic nanoparticles: review of synthesis methods, surface functionalization approaches, and biomedical applications, Nanotechnol. Rev., 2018, 7(2), 187-207.

[15] Hong R.Y., Pan T.T., Qian J.Z., Li H.Z., Synthesis and surface modification of ZnO nanoparticles, Chem. Eng. J., 2006, 119(2), 71-81.

[16] Zhang W., Shen F.L., Hong R.Y., Solvothermal synthesis of magnetic Fe_3O_4 microparticles via self-assembly of Fe_3O_4 nanoparticles, Particuology., 2011, 9(2), 179-186.

[17] Das S., Srivastava V.C., An overview of the synthesis of CuO-ZnO nanocomposite for environmental and other applications, Nanotechnol. Rev., 2018, 7(3), 267-282.

[18] Tang X., Hong R.Y., Feng W.G., Badami D., Ethylene glycol assisted hydrothermal synthesis of strontium hexaferrite nanoparticles as precursor of magnetic fluid, J. Alloys Compd., 2013, 562, 211-218.

[19] Liu J.R., Hong R.Y., Feng W.G., Badami D., Wang Y.Q., Large-scale production of strontium ferrite by molten-salt-assisted coprecipitation, Powder Technol., 2014, 262, 142-149.

[20] Low F. W., Lai, C. W., Abd Hamid, S. B., Easy preparation of ultrathin reduced graphene oxide sheets at a high stirring speed, Ceram. Int., 2015, 41(4), 5798-5806.

[21] Durmus Z., Kavas H., Durmus A., Aktaş B., Synthesis and microstructural characterization of graphene/strontium hexaferrite ($SrFe_{12}O_{19}$) nanocomposites, Mater. Chem. Phys., 2015, 163, 439-445.

[22] Ding Y., Zhang L., Liao Q., Zhang G., Liu S., Zhang Y., Electromagnetic wave absorption in reduced graphene oxide functionalized with Fe_3O_4/Fe nanorings, Nano Res., 2016, 9(7), 2018-2025.

[23] Zhang T., Peng X., Li, J., Yang Y., Xu J., Wang P., Jin D., Jin H., Hong B., Wang X., Ge H., Platelet-like hexagonal $SrFe_{12}O_{19}$ particles: hydrothermal synthesis and their orientation in a magnetic field, J. Magn. Magn. Mater., 2016, 412, 102-106.

[24] Yao Y., Miao S., Liu S., Ma L.P., Sun H., Wang S., Synthesis, characterization, and adsorption properties of magnetic Fe_3O_4@graphene nanocomposite, Chem. Eng. J., 2012, 184, 326-332.

[25] Shafiu S., Sözeri H., Baykal A., Solvothermal synthesis of $SrFe_{12}O_{19}$ hexaferrites: without calcinations, J. Supercond. Novel Magn., 2014, 27(6), 1593-1598.

[26] Cheng Y., Cao J., Li Y., Li Z., Zhao H., Ji G., Du Y., The outside-In approach to construct Fe_3O_4 nanocrystals/mesoporous carbon hollow spheres core–shell hybrids toward microwave absorption, ACS Sustainable Chem. Eng., 2017, 6(1), 1427-1435.

[27] Cheng Y., Cao J., Li Y., Li Z., Zhao H., Ji G., Du Y., The outside-In approach to construct Fe_3O_4 nanocrystals/mesoporous carbon hollow spheres core–shell hybrids toward microwave absorption, ACS Sustainable Chem. Eng., 2017, 6(1), 1427-1435.

[28] Chen Y.H., Huang Z.H., Lu M.M., Cao W.Q., Yuan J., Zhang D.Q., Cao,M.S., 3D Fe_3O_4 nanocrystals decorating carbon nanotubes to tune electromagnetic properties and enhance microwave absorption capacity, J. Mater. Chem. A., 2015, 3(24), 12621-12625.

[29] Chelliah C.R.A.J., Swaminathan R., Current trends in changing the channel in MOSFETs by III-V semiconducting nanostructures, Nanotechnol. Rev., 2017, 6(6), 613-623.

[30] Liu P.B., Huang Y., Zhang X., Cubic $NiFe_2O_4$ particles on graphene-polyaniline and their enhanced microwave absorptionproperties, Compos. Sci. Technol., 2015, 107, 54-60.

[31] Xu D., Xiong X., Chen P., Yu Q., Chu H., Yang S., Wang Q., Superior corrosion-resistant 3D porous magnetic graphene foam-ferrite nanocomposite with tunable electromagnetic wave absorption properties, J. Magn. Magn. Mater., 2019, 469, 428-436.

[32] Cheng Y., Li Z.Y., Li Y., Dai S.S., Ji G.B., Zhao H.Q., Gao J.M., Du Y.W., Rationally regulating complex dielectric parameters of mesoporous carbon hollow spheres to carry out efficient microwave absorption, Carbon., 2018, 127, 643-652.

[33] Rusly S.N.A., Ismail I., Matori K.A., Abbas Z., Shaari A.H., Awang Z., Ibrahim I.R., Idris F.M., Zaid M.H.M., Mahmood K.A., Hasan I.H., Influence of different BFO filler content on microwave ab-

sorption performances in $BiFeO_3$/epoxy resin composites, Appl. Surf. Sci., 2020, 46(1), 717-746.

[34] Shen W., Ren B., Wu S., Wang W., Zhou X., Facile synthesis of rGO/$SmFe_5O_{12}$/$CoFe_2O_4$ ternary nanocomposites: Composition control for superior broadband microwave absorption performance, Appl. Surf. Sci., 2018, 453, 464-476.

[35] Wu N., Xu D., Wang Z., Wang F., Liu J., Liu W., Shao Q., Liu H., Gao Q., Guo Z., Achieving superior electromagnetic wave absorbers through the novel metal-organic frameworks derived magnetic porous carbon nanorods, Carbon., 2019, 145, 433-444.

[36] Ma J., Shu J., Cao W., Zhang M., Wang X., Yuan J., Cao M., A green fabrication and variable temperature electromagnetic properties for thermal stable microwave absorption towards flower-like Co_3O_4@rGO/SiO_2 composites, Compos. Part. B-Eng., 2019, 166, 187-195.

[37] Liu P., Zhang Y., Yan J., Huang Y., Xia L., Guang Z., Synthesis of lightweight N-doped graphene foams with open reticular structure for high-efficiency electromagnetic wave absorption, Chem. Eng. J., 2019, 368, 285-298.

[38] Chen W., Liu Q., Zhu X., Fu M., One-step in situ synthesis of strontium ferrites and strontium ferrites/graphene composites as microwave absorbing materials, RSC Adv., 2017, 7(64), 40650-40657.

[39] Song C.Q., Yin X.W., Han M.K., Li X.L., Hou Z.X., Zhang L.T., Cheng L.F., Three-dimensional reduced graphene oxide foam modified with ZnO nanowires for enhanced microwave absorption properties, Carbon., 2017, 116, 50-58.

[40] Ye F., Song Q., Zhang Z.C., Li W., Zhang S.Y., Yin X.W., Zhou Y.Z., Tao H.W., Liu Y.S., Cheng L.F., Direct growth of edge-rich graphene with tunable dielectric properties in porous Si_3N_4 ceramic for broadband high-performance microwave absorption, Adv. Funct. Mater., 2018, 28(17), 1707205.

[41] Liang K., Qiao X.J., Sun Z.G., Guo X.D., Wei L., Qu Y., Preparation and microwave absorbing properties of graphene oxides/ferrite composites, Appl. Phys. A., 2017,123(6),445.

[42] Wang Y.M., Luo Z., Hong R.Y., Microstructure and microwave absorption properties of Fe_3O_4/dextran/SnO_2 multilayer microspheres, Mater. Lett., 2011, 65 (21), 3241-3244.

[43] Han Q., Meng X., Lu C., Exchange-coupled $Ni_{0.5}Zn_{0.5}Fe_2O_4$/$SrFe_{12}O_{19}$ composites with enhanced microwave absorption performance, J. Alloys Compd., 2018, 768, 742-749.

[44] Yang Y., Xia L., Zhang T., Shi B., Huang L., Zhon, B., Zhang X., Wang H., Zhang J., Wen G., Fe_3O_4@LAS/RGO composites with a multiple transmission-absorption mechanism and enhanced electromagnetic wave absorption performance, Chem. Eng. J., 2018, 352, 510-518.

[45] Wang Y., Wu X.M., Zhang W.Z., Luo C.Y., Li J.H., Wang Y.J., Fabrication of flower-like $Ni_{0.5}Co_{0.5}(OH)_2$@PANI and its enhanced microwave absorptionperformances, Mater. Res. Bull., 2018, 98,59-63.

[46] Liu Q.H., Gao Q., Bi H., Liang C.Y., Yuan K.P., She W., Yang Y.J., Che R.C., CoNi@SiO_2@TiO_2 and CoNi@Air@TiO_2 microspheres with strong wideband microwave absorption, Adv. Mater., 2016, 28(3), 486-490.